# Superconducting electron and hole lenses

H. Cheraghchi,[1] H. Esmailzadeh,[2] and A. G. Moghaddam[2,*]
[1]*School of Physics, Damghan University, Damghan 36716-41167, Iran*
[2]*Department of Physics, Institute for Advanced Studies in Basic Sciences (IASBS), Zanjan 45137-66731, Iran*
(Received 10 January 2016; revised manuscript received 12 May 2016; published 16 June 2016)

We show how a superconducting region (S), sandwiched between two normal leads (N), in the presence of barriers, can act as a lens for propagating electron and hole waves by virtue of the so-called crossed Andreev reflection (CAR). The CAR process, which is equivalent to Cooper pair splitting into two N electrodes, provides a unique possibility of constructing entangled electrons in solid state systems. When electrons are locally injected from an N lead, due to the CAR and normal reflection of quasiparticles by the insulating barriers at the interfaces, sequences of electron and hole focuses are established inside another N electrode. This behavior originates from the change of momentum during electron-hole conversion beside the successive normal reflections of electrons and holes due to the barriers. The focusing phenomena studied here are fundamentally different from the electron focusing in other systems, such as graphene *p-n* junctions. In particular, due to the electron-hole symmetry of the superconducting state, the focusing of electrons and holes is robust against thermal excitations. Furthermore, the effects of the superconducting layer width, the injection point position, and barrier strength are investigated on the focusing behavior of the junction. Very intriguingly, it is shown that by varying the barrier strength, one can separately control the density of electrons or holes at the focuses.

DOI: 10.1103/PhysRevB.93.214508

## I. INTRODUCTION

One of the fundamental aspects of quantum mechanics is nonlocality which manifests as nonclassical correlations between spatially separated particles, which is usually referred to as quantum entanglement [1]. During the last decades tremendous efforts have concentrated on exploiting entanglement as the main resource for quantum information processing and its technological applications [2]. In solid state systems, among a variety of proposed methods to create entanglement between electrons, one of the most accessible sources of entangled electrons is Cooper pair (CP) splitting [3,4]. In conventional superconductors, CPs are composed of two electrons in a spin singlet state which can be used to produce two entangled electrons. The process of spatially separating two electrons of a CP without losing their correlations is commonly referred to as crossed Andreev reflection (CAR), which takes place in a system of a superconductor (S) coupled to two normal leads (N) [5–10]. In this process an incoming electron from one N lead is able to enter the S region via attracting another electron from the other N lead, which leaves a hole inside it.

Unlike Andreev reflection (AR), which takes place locally at any NS interface, CAR has been proved to be hardly detectable in experiments, due to the cancellation of its contribution with that of elastic cotunneling (EC) in cross conductance measurements [11–14]. Among the proposed setups to detect CAR, one method which has been experimentally verified uses two quantum dots between each N lead and the superconductor [15–19]. In other proposals, the replacement of normal leads with strong ferromagnets (F) or even a spin half metal has been suggested [20–22]. Alternatively, some other works have focused on the diffusive regime of transport in NSN structures [23–25]. Other groups have revealed that the Coulomb interactions, in particular, in quantum dot systems, can lead to nonlocal Andreev processes [26,27]. Moreover, very recently it has been suggested to use devices based on graphene or topological insulators and generally two-dimensional materials in which low-energy excitations behave as Dirac fermions [28–34].

In this paper we investigate the focusing effect for both electrons and holes injected locally from an electron source and passing through a planar normal-insulator-superconductor-insulator-normal (NISIN) junction. The transport properties of such ballistic systems and particularly the effect of barriers on CAR and EC signals have been already investigated [8–10]. Here, we will show any planar ballistic NISIN junction under certain circumstances can lead to the focusing of both electrons and holes. The underlying mechanism for the focusing property here is the combination of CAR or equivalently nonlocal electron-hole conversion (EHC) induced by superconducting correlations with large momentum transfer due to the potential barriers at the interfaces. The main characteristic of NISIN junctions is depicted schematically in Fig. 1, where some semiclassical trajectories of electrons and holes originating from a point source are shown. It clearly shows that electron and hole trajectories are completely separated since the momentum and velocity directions for electron and hole excitations are parallel and antiparallel, respectively. When electronic waves injected from a point source inside $N_1$ arrive at an NS interface, they are partially reflected and transmitted as both electrons and holes where the last scattering process occurs due to EHC. In other words, there exist four different scattering processes in NISIN junctions, including normal and Andreev reflections which take place locally, as well as EC and CAR which correspond to the transmission as an electron and a hole, respectively. In particular, for the transmitted waves each EHC process results in a negative refraction of electronic wave functions and then successive scattering processes can

*agorbanz@iasbs.ac.ir

 

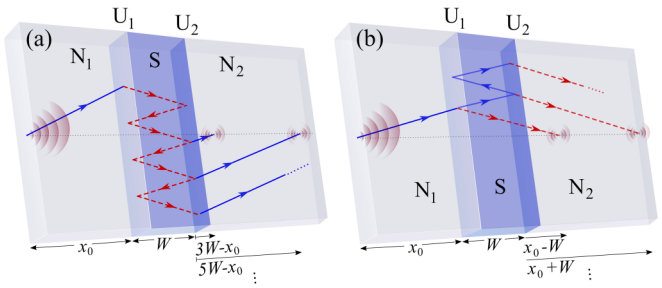


FIG. 1. A schematic view of the superconducting lens is shown beside the classical trajectories of electrons (solid blue lines) and holes (dashed red lines) originating from a point source inside $N_1$. The focusing effect is caused by the crossed Andreev reflection (nonlocal electron-hole conversion) in combination with normal reflections which take place at the interfaces. It must be noticed that, for clarity, only the trajectories with a certain angle are shown. However, according to the conservation rules and simple geometric relations, the positions of focal points where the trajectories cross the $x$ axis do not change by varying the angle.

give rise to a sequence of electron and hole focal points inside $N_2$ (see Fig. 1).

It must be mentioned that prior to the present work, Gómez *et al.* have shown that an NSN junction based on graphene can act as a lens for electron and hole excitations [35]. However, in their investigation the lensing property is mostly accompanied by the chiral relativistic characteristics of the charge carriers and the so-called Klein tunneling which occurs at $p$-$n$ type interfaces in graphene. In fact, even without the superconducting correlations, Dirac systems such as graphene have been proven to show negative refraction at the $p$-$n$ interfaces and they can behave as Veselago-like lenses [36,37]. On the other hand, here we show that in NISIN junctions, the combination of EHC with the effect of barriers can lead to electron and hole focusing. This phenomenon does not require a special Dirac band structure of graphene or topological insulators, and it can be in principle observed in conventional superconducting devices as well as those based on Dirac materials.

The paper is organized as follows. After the introduction, in Sec. II, the model consisting of a superconductor between normal metals and in the presence of barriers is introduced. The formulation, which is based on the Gorkov's equations and Green's functions, is presented afterwards. In Sec. III we show the numerical results for local particle and current densities. These results reveal the electron and hole focusing phenomena in the NISIN structure. Our findings are followed by a discussion on the basic underlying mechanisms, the effects of various parameters and irregularities on the results, and possible experimental realizations. Finally, Sec. IV is devoted to the conclusions.

## II. THEORETICAL MODEL AND FORMALISM

In order to have a quantitative description of the anticipated focusing effects in NISIN junctions, we exploit the Green's function formalism. In superconducting structures and for the time-independent situations, the full Green's function $\hat{\mathcal{G}}(\mathbf{r},t|\mathbf{r}',t') = \int d\omega \hat{\mathcal{G}}_\omega(\mathbf{r}|\mathbf{r}') \exp[-i\omega(t-t')]$ is defined with the following matrix form in the Nambu space and the energy representation,

$$\hat{\mathcal{G}}_\omega(\mathbf{r}|\mathbf{r}') = \begin{pmatrix} g(\mathbf{r}|\mathbf{r}';\omega) & f(\mathbf{r}|\mathbf{r}';\omega) \\ f^\dagger(\mathbf{r}|\mathbf{r}';\omega) & -g(\mathbf{r}'|\mathbf{r};\omega) \end{pmatrix}, \tag{1}$$

in which

$$g(\mathbf{r}|\mathbf{r}';\omega) = \int d\tau e^{i\omega\tau} \langle \hat{\psi}_s^\dagger(\mathbf{r},\tau)\hat{\psi}_s(\mathbf{r}',0)\rangle, \tag{2}$$

$$f(\mathbf{r}|\mathbf{r}';\omega) = -\int d\tau e^{i\omega\tau} \langle \hat{\psi}_\uparrow(\mathbf{r},\tau)\hat{\psi}_\downarrow(\mathbf{r}',0)\rangle, \tag{3}$$

are the so-called normal and anomalous parts of the Green's function. Here, field operators $\hat{\psi}_s^\dagger(\mathbf{r},\tau)$ and $\hat{\psi}_s(\mathbf{r},\tau)$ represent the creation and annihilation of excitations with spin $s$ at point $\mathbf{r}$ and time $\tau$. The statistical averaging is denoted by $\langle\cdots\rangle$. In the ballistic regime, the full Green's function can be obtained from the matrix form of the Gorkov equations [38],

$$[\omega - \mathcal{H}(\mathbf{r})\hat{\tau}_z + \Delta(\mathbf{r})\hat{\tau}_x - \hat{\mathcal{V}}_{\rm ext}]\hat{\mathcal{G}}_\omega(\mathbf{r}|\mathbf{r}') = \delta(\mathbf{r}-\mathbf{r}'), \tag{4}$$

with Pauli matrices $\hat{\tau}_z$ and $\hat{\tau}_x$ operating over the Nambu (electron-hole) space. The single particle Hamiltonian $\mathcal{H}(\mathbf{r})$ describes a typical metal with a quadratic dispersion relation as

$$\mathcal{H}(\mathbf{r}) = -\frac{\hbar^2}{2m}\nabla^2 + \mathcal{U}(\mathbf{r}) - \mu, \tag{5}$$

in which $\mu$ indicates the Fermi energy. For the superconducting gap we use the sharp interface model in which the gap has a constant finite value $\Delta(\mathbf{r}) = \Delta_0$ inside the superconductor ($0 < x < W$) and vanishes outside it. In fact, the more precise spatial form of the pair potential should be obtained using the self-consistency relation of the gap $\Delta(\mathbf{r}) = -\lambda \int d\omega f(\mathbf{r}|\mathbf{r};\omega)$. However, due to the presence of barriers at the interfaces, the superconducting gap inside S is only weakly affected by the adjacent N regions and therefore using a self-consistency equation to obtain the spatial variations of $\Delta(\mathbf{r})$ is not crucial. The potential function $\mathcal{U}(\mathbf{r}) = [U_1\delta(x-0) + U_2\delta(x-W)]W$ accounts for the two barriers at the interfaces induced by atomically thin insulating layers. In the absence of an external potential which represents the electron injection, the Gorkov equation can be solved to obtain the unperturbed Green's function $\hat{\mathcal{G}}_0(\mathbf{r}|\mathbf{r}')$. Then, in the presence of external perturbation $\hat{\mathcal{V}}_{\rm ext}(V_0/2)(\hat{\mathbb{1}} + \hat{\tau}_z)\delta(\mathbf{r}-\mathbf{r}_0)$, the full Green's function $\hat{\mathcal{G}}(\mathbf{r}|\mathbf{r}')$ can be obtained using the Dyson equation,

$$\hat{\mathcal{G}}(\mathbf{r}|\mathbf{r}') = \hat{\mathcal{G}}_0(\mathbf{r}|\mathbf{r}') + \int d\mathbf{x}\, \hat{\mathcal{G}}_0(\mathbf{r}|\mathbf{x})\hat{\mathcal{V}}_{\rm ext}(\mathbf{x})\hat{\mathcal{G}}(\mathbf{x}|\mathbf{r}'). \tag{6}$$

From the Green's function one can calculate all of the local properties of the system, including local densities and currents in the framework of linear response theory. In particular, the electron and hole local density of states (LDOS) can be extracted from the diagonal components of matrix $\hat{\mathcal{G}}_\omega(\mathbf{r}|\mathbf{r})$, namely, using the relations $n_e(\mathbf{r};\omega) = \mathrm{Im}\,\mathcal{G}_\omega^{ee}(\mathbf{r}|\mathbf{r})$ and $n_h(\mathbf{r};\omega) = \mathrm{Im}\,\mathcal{G}_\omega^{hh}(\mathbf{r}|\mathbf{r})$. Then, assuming weak electron

injection from the source at $\mathbf{r}_0$ and expanding over $V_0$, the lowest-order corrections of the electrons and holes LDOS read

$$\delta n_e(\mathbf{r};\omega) \propto \mathrm{Im}[g_0(\mathbf{r}|\mathbf{r}_0;\omega)g_0(\mathbf{r}_0|\mathbf{r};\omega)], \tag{7}$$

$$\delta n_h(\mathbf{r};\omega) \propto \mathrm{Im}[f_0^\dagger(\mathbf{r}|\mathbf{r}_0;\omega)f_0(\mathbf{r}_0|\mathbf{r};\omega)], \tag{8}$$

where $g_0$ and $f_0$ indicate the normal and anomalous parts of the unperturbed Green's function. On the same ground one can immediately see that the magnitudes of local current densities, up to linear order in the injected current at the source point, are given by

$$J_e(\mathbf{r};\omega) \propto |g_0(\mathbf{r}|\mathbf{r}_0;\omega)g_0(\mathbf{r}_0|\mathbf{r};\omega)|, \tag{9}$$

$$J_h(\mathbf{r};\omega) \propto |f_0^\dagger(\mathbf{r}|\mathbf{r}_0;\omega)f_0(\mathbf{r}_0|\mathbf{r};\omega)|. \tag{10}$$

## III. NUMERICAL RESULTS AND DISCUSSION

In the following, we will present the numerical results obtained by a discretized Green's function calculation for LDOS and current densities. Using the translational symmetry along the vertical $y$ direction, the unperturbed Green's function can be written in the Fourier transformed form,

$$\hat{\mathcal{G}}_0(\mathbf{r}|\mathbf{r}') = \int \frac{dq}{2\pi} e^{-iq(y-y')}\hat{\mathcal{G}}_0(x|x';q). \tag{11}$$

Hence, Eq. (4) reduces to a one-dimensional form for $\hat{\mathcal{G}}_0(x|x';q)$ which can be solved in general by discretization methods. The only important point is to set the increment $\delta x$ small enough in comparison to the Fermi wavelength $\lambda_F$, which is the smallest length scale of the problem. Finally, by numerical implementation of the two integrations in Eqs. (11) and (6), the perturbed Green's function at the presence of the electron source can be obtained.

In order to have an observable CAR signal, the superconductor must have a width $W$ comparable with the superconducting coherence length $\xi = \hbar v_F/\Delta_0$ in which $v_F$ is the Fermi velocity [10]. In fact, the nonlocal EHC is efficient only when $W \sim \xi$, which increases the probability of CAR. For thinner or very wide superconducting layers the CAR is weakened in favor of EC and local AR, respectively. In typical superconductors with $\Delta_0 \lesssim 1$ meV, the superconducting correlations extend over $\xi \sim 0.1$–$1$ $\mu$m, which gives the typical size of the proposed superconducting lenses. In addition, the presence of potential barriers at the interfaces $x = 0, W$ leads to a further suppression of the local AR and EC through the junction and subsequently increases the efficiency of electron or hole wave focusing mediated by a combination of CAR and normal reflections from the barriers.

In the following, the electron and hole focusing property of a superconducting NISIN heterostructure is examined by studying the spatial variations of the induced local density and local currents inside the second N region. We further investigate the influence of the width of the superconducting region, the distance of the electron injection from the interfaces, and the strength of the barriers at the interfaces on the focusing properties of the superconducting lens. Finally, we comment on the experimental feasibility of the theoretical model and discuss the obtained results and their limitations.

### A. Electron and hole focusing

In order to see the focusing signature of the superconducting layer, the spatial variations of the LDOS for the electrons and holes are shown in Fig. 2. We define the dimensionless excess density of states denoted by $\widetilde{\delta n}(\mathbf{r}) = \delta n(\mathbf{r})/(V_0 n_0^2)$ in which $n_0 = m/(\pi\hbar^2)$ is the constant density of states of the two-dimensional electron gas (2DEG). The width of the S layer is assumed to be $W = 0.5\xi$ and the source is placed at $x_0 = -2.7W$. Now the sequences of the focal points where electrons and holes are focused can be clearly seen in Fig. 2. These focal points are accompanied by oscillations around them which originate from the quantum interference of refracted electronic waves. In the case of electron density due to the EC, there is an extra overall push function which shows decreasing oscillatory dependence with the distance from the second interface. On the other hand, the focuses followed by oscillations around them can be seen in the hole density. As we will discuss in the following, the focuses of either electrons or holes originate from the combination of EHC at the N/S interfaces and normal reflection of Bogoliubov quasiparticles inside the superconductor. It must be emphasized that the second process is only possible when the barriers are present. Moreover, without any barrier at the interfaces the CAR itself will be suppressed in favor of the AR and EC processes.

It is instructive to describe the appearance of electron and hole focuses based on a semiclassical argument. As illustrated in Fig. 1, the trajectories of propagating electronic waves, originating from the injection point $x_0$ inside $N_1$, are refracted at the N/S interfaces when an EHC takes place. It is well known that the holes, as excitations below the Fermi

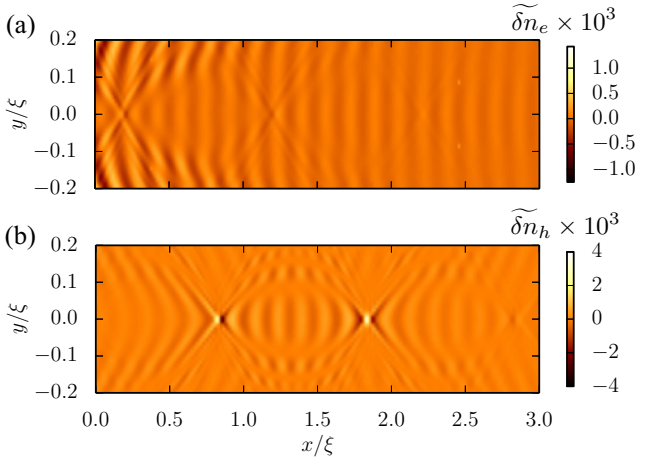


FIG. 2. Spatial variations of (a) electron and (b) hole scaled excess densities defined by $\widetilde{\delta n} = \delta n/(V_0 n_0^2)$. The electron injector is located at $x_0 = -2.7W$ inside the first N lead, measured from the first interface. The density profiles are plotted inside the second normal contact $N_2$. The superconducting layer has a width $W = 0.5\xi$ and the potential barriers at the interfaces are $U_1 = U_2 = 2\mu$ and other parameters are $\Delta_0/\mu = 0.01$, $\epsilon/\Delta_0 = 0.8$. For both electron and hole sequences the focal points along the $x$ axis can be observed. The electron density shows an extra decaying push which indicates the EC contributions. The oscillations in the densities are due to the quantum interference of electronic waves upon scattering from the interfaces and the superconducting layer.

level, have momentum and velocity with opposite directions. However, the velocity and momentum of the electrons have the same direction. Therefore, when an EHC occurs, because of momentum conservation along the $y$ direction, the electronic waves undergo a negative refraction which is revealed in the classical trajectories as well. The negative refraction here is reminiscent of the famous Veselago lenses in optics which are made at the interfaces between a conventional dielectric medium and a metamaterial with a negative refraction index. Now the refractions caused by EHC and successive normal reflections of the Bogoliubov quasiparticles from the barriers can result in a sequence of focuses inside the lead $N_2$. It should be noticed that the presence of barriers is not only crucial for normal reflections but also they provide the source of the large momentum transfer in the EHC processes. In Fig. 1, for the sake of clarity, only those trajectories which lead to a focal point are shown. However, there are other trajectories corresponding to the normal and Andreev reflections back into $N_1$ as well as the diverging waves of electrons and holes inside $N_2$, which are not shown here.

The semiclassical trajectories of electrons and holes can be helpful in finding the positions of the focal points. It must be mentioned that although the trajectories are defined by both the source point and the angle of incidence, however, the positions of the focuses do not vary by the angle of trajectories, warranted by the simple trigonometric relations. Depending on the number of EHCs during a process (being even or odd), an electron or a hole focus shows up, which can be seen from Figs. 1(a) and 1(b), respectively. When the number of normal reflections back into the superconductor increases, new focuses far from the second interface can be established. Then, in principle, we end up with two infinite sequences of separate electron and hole focuses. Using the trigonometric relations, the positions of the electron and hole focuses are obtained as below,

$$\begin{aligned} x_e^{(n)} &= (2n+1)W - x_0, \\ x_h^{(n)} &= (2n-1)W + x_0, \quad n = 0,1,2,\ldots. \end{aligned} \tag{12}$$

One should note that the first electron focus corresponds to $n_{e;1} = \lfloor (x_0/2W) + 0.5 \rfloor$ while the hole focuses start from $n_{h;1} = 1$ or 0 depending on the width $W$ being larger or smaller than $x_0$, respectively.

### B. Electron and hole local current densities

Very similar to the LDOS, the local current densities of electrons and holes denoted by $J_e$ and $J_h$ can indicate the focusing signature of the superconducting layer between two normal electrodes. The intensities of electron and hole currents with the corresponding focal points are shown in Fig. 3. There are also small oscillations around the focuses but not as clear as the Friedel-type oscillations revealed in the LDOS spatial variations. Here, a single geometry but for different configurations of the barriers is considered, in order to see the effect of the barriers more clearly. Figures 3(a)–3(c) correspond to the cases with two barriers, a single barrier at the first interface, and finally a single barrier at the second interface with corresponding sketches for the electron and hole trajectories. We see that in the presence of both barriers

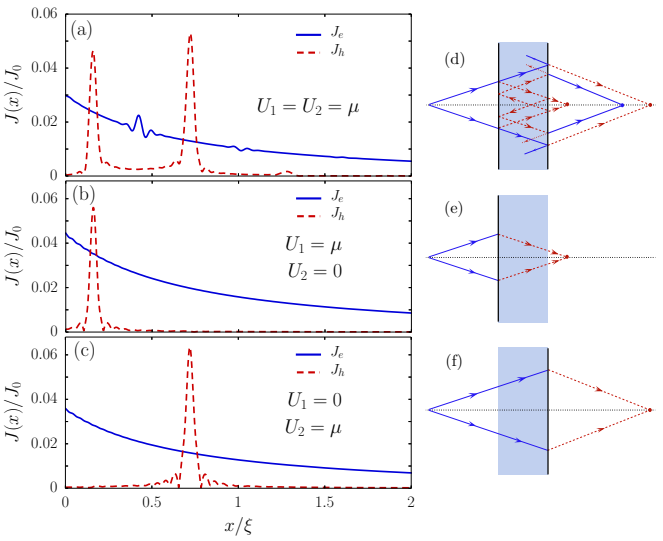


FIG. 3. Local current densities of electrons ($J_e$) and holes ($J_h$) inside $N_2$ along the $x$ axis and vs the distance from the second interface when (a) $U_1 = U_2 = \mu$, (b) $U_1 = \mu, U_2 = 0$, and (c) $U_1 = 0$ and $U_2 = \mu$. (d)–(f) indicate the corresponding schematics in which the classical trajectories leading to the electron and hole focuses are shown. The electron and hole propagations are indicated by solid blue and dashed red lines, respectively. The width of the superconductor and injection point position are $W/\xi = 0.22$ and $x_0/\xi = 0.35$. The superconducting gap and excitation energy are assumed as $\Delta_0/\mu = 0.01$ and $\epsilon/\Delta_0 = 0.8$. This figure clearly indicates that the sequence of focuses can be observed when both interfaces have a limited transparency ($U \neq 0$). However, when the second or first interfaces are fully transparent ($U = 0$), only the first and second hole focuses survive, respectively.

the first two focuses of the holes are very strong. These two focal points correspond respectively to the EHC at the first and second interfaces. Other focuses for the holes as well as those of electrons are much weaker since they originate from higher-order processes when successive EHC and normal reflections take place. When one of the barriers is absent, then the normal reflections cannot lead to further focuses. Subsequently, the EHC is sufficiently strong only at one of the interfaces, which leads to a single hole focus without any electron focusing. This suggests a way to control the intensity of different focuses by varying the strength of the two barriers, separately.

As mentioned earlier, the CAR is very effective for S layers with a certain range of widths being on the order of the coherence length ($W \sim \xi$). Hence, we expect that varying the width of the S layer can strongly influence the focusing properties. This can be seen clearly in Fig. 4, where the spatial variations of the electron and hole local currents for various values of $W/\xi$ are shown. Starting from a thin S layer with $W/\xi = 0.2$, EC processes are dominant and therefore the overall push of the electron current is larger, as indicated in Fig. 4(a). By increasing the width, the EC signal weakens, and due to the dominance of CAR, the electron and hole focuses are more intense for the junctions with intermediate widths, e.g., $W/\xi = 0.5$. Then a further increase in the width weakens the CAR in favor of local AR and subsequently

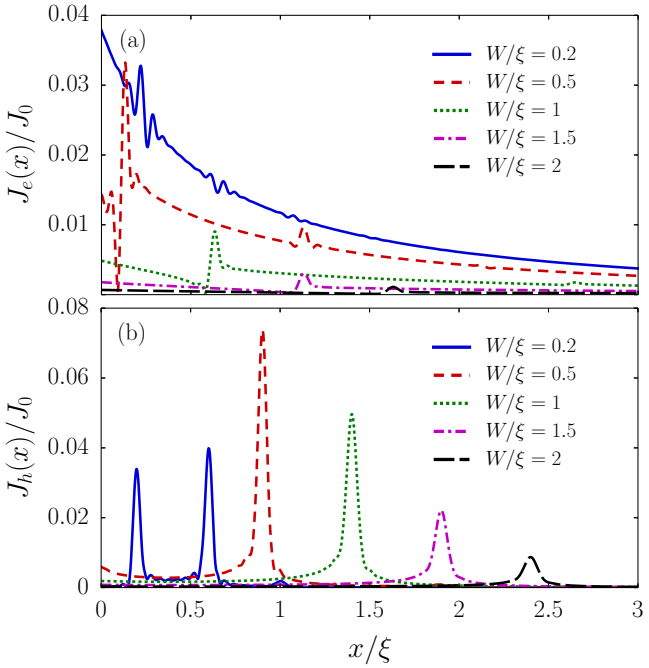


FIG. 4. Spatial variation of the local current densities for (a) electrons and (b) holes vs the distance from the second interface along the $x$ axis for various values of the superconducting layer width $W$. Although the EC signal indicated by electron current $J_e$ shows an overall decline for wider $W$, the CAR signal given by hole current $J_h$ is strong for $W/\xi \lesssim 1$. The parameters used for this plot have the values $x_0/\xi = 0.4$, $U_1 = U_2 = \mu$, $\lambda_F/\xi = 0.04$, and $\epsilon/\Delta_0 = 0.8$.

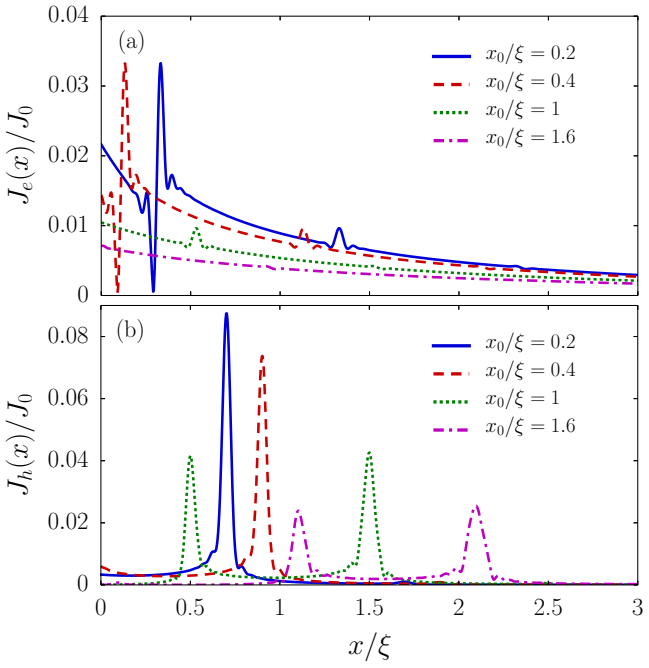


FIG. 5. Spatial variation of (a) local electron current and (b) hole current along the $x$ axis for various distances of the injection point from the first interface ($x_0$). The width of the superconductor is $W/\xi = 0.5$ and other parameters are the same as those in Fig. 4.

the intensity of the currents and excess densities around the focuses will be suppressed. For very long junctions $W \gg \xi$ only normal reflection and AR could take place and CAR as well as the focusing signature diminish. As another interesting point it must be mentioned that when the width of the junction is smaller than the distance of the injection point from the first interface ($x_0$), two first hole focuses are very intense. These focuses originate from the EHC at the first and second interfaces, respectively, and their positions are $x_h^{(0)} = x_0 - W$ and $x_h^{(1)} = x_0 + W$, according to Eq. (12). On the other hand, when the width is larger than the distance $x_0$, the EHC at the first interface cannot give rise to a hole focus inside $N_2$, as can be understood from Fig. 1(b). Therefore, only one single hole focus located at $x_h^{(1)}$ becomes intense when $W > |x_0|$. Other hole focuses with $n_h \geqslant 2$ as well as those of electrons which are related to the higher-order processes have much weaker intensities, as explained before.

To see the effect of the injection point distance on the EC and CAR signals, Fig. 5 shows the spatial variations of $J_e$ and $J_h$ for some different values of $x_0/\xi$ when the width is $W = 0.5\xi$. The results show that both electron and hole currents with main contributions from EC and CAR decrease if the injection point becomes farther away from the S layer. Moreover, as it has been mentioned above, depending on the distance of the injection point being smaller or larger than $W$, there will be a single or two intense hole focuses, respectively. On the same ground, when the injection point is close to the S layer ($|x_0| < W$), the first electron focus which originates from two successive EHCs at the two interfaces is very strong. However, in the opposite limit of far injection points ($x_0 > W$), besides EHC processes, two or more reflections of Bogoliubov excitations from the interfaces back into the S layer take place to establish the first electron focusing. Therefore, the intensity of the resulting electron focuses will be much weaker, as it is clear from Fig. 5(a).

Before closing this part, we should comment on the effect of the excitation energy $\epsilon$ on the focusing properties of the NISIN junctions. Throughout the paper the results are presented for a certain value of energy inside the superconducting gap, $\epsilon = 0.8\Delta_0$. However, we have checked the dependence of the results on $\epsilon$ and it has been found that the change in the excess densities $\delta n_{e,h}$ and currents $J_{e,h}$ due to the excitation energy being varied from 0 to $\Delta_0$ is very small. This is a simple consequence of the fact that the superconducting gap and therefore $\epsilon$ is very much smaller than the Fermi energy $\mu$ and all of the wave vectors $k_{e,h} = \sqrt{(2m/\hbar^2)(\mu \pm \epsilon)}$ can be approximated with $k_F = \sqrt{(2m/\hbar^2)\mu}$. So the scattering and focusing properties of the junction are determined only by the geometrical parameters $W$ and $x_0$ as well as the Fermi wave vector, almost irrespective of the excitation energy. Above the superconducting gap ($\epsilon > \Delta_0$) the EHC is suppressed and subsequently the focusing patterns disappear when $\epsilon \gg \Delta_0$.

### C. The effect of barrier strength

In what follows, we examine the influence of the barrier strength in more detail. As it has been revealed by our above results, the presence of at least one potential barrier at the interfaces is crucial for the emergence of hole focusing. On the other hand, the electron focusing will be absent unless

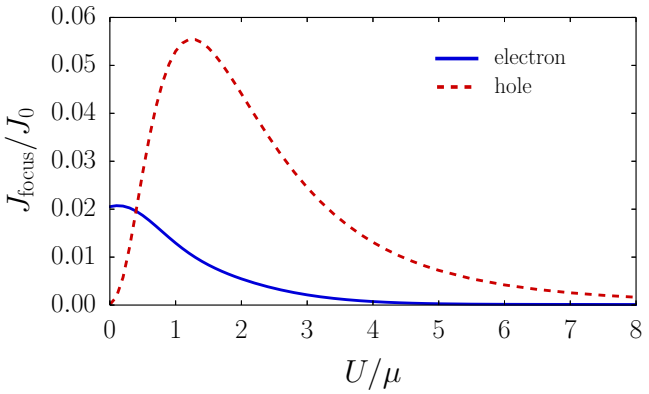


FIG. 6. Dependence of the hole and electron current densities at the first hole focus ($x_h^{(0)}$) on the barrier strength $U$. Although the electron current decreases monotonically with $U$, the hole current at the focus becomes maximum at a certain strength of the potential barrier $U/\mu \sim 1$. All the parameters used here are the same as in Fig. 3(a).

we have effective barriers at both interfaces. In the absence of potential barriers, the dominant scattering processes are AR and EC, where both satisfy the momentum conservation. The presence of barriers at the interfaces favors the normal reflection and CAR, which involve a finite momentum transfer and simultaneously suppress the other scattering processes, i.e., local AR and EC.

Now, as one can see from Fig. 6, when potential barriers are very weak ($U \ll \mu$), which leads to very transparent interfaces, CAR and the intensity of focusing are negligibly small. By increasing the potential strength, the EHC and resulting CAR become more effective at the intermediate values $U \sim \mu$. Nevertheless, for very strong barriers, the competition between normal reflection and CAR is in favor of the first process. Therefore, the intensity of the local hole current around the focuses declines by a further increase in the barrier strength and becomes fully suppressed for $U \gg \mu$. Unlike the hole current, which reveals a maximum value around $U \sim \mu$, the electron local current, originating from EC, monotonically decreases with $U$, in particular, in the regime of strong barriers ($U > \mu$).

### D. On the experimental feasibility

As it has been already mentioned, we show that a generic superconducting NISIN heterostructure can focus both electrons and holes. Moreover, the focusing property of the junction is irrespective of the band structure and dispersion relation of the normal leads and the superconductor. In fact, there is no need for a special band structure or other features, such as the Dirac spectrum considered in previous studies [35]. Then devices based on conventional systems such as 2DEG as well as graphene and other 2D materials can be used as the normal leads contacted to a superconducting region at the middle to see the lensing phenomena for electrons and holes.

Although the specific band structure is not an important requirement for the superconducting lens studied here, it should be noticed that this electronic lens could work properly under certain circumstances. Nevertheless, we will discuss that these requirements can be fulfilled in currently available experimental setups, and subsequently our predictions can be checked experimentally. First of all, we assume that the Fermi velocities inside the normal and superconducting regions are almost equal to each other. Fortunately, this assumption can be essentially satisfied in the common superconducting heterostructures based on metals, semiconductors, and even structures based on graphene and topological insulators [39,40]. Another important requirement is the presence of effective potential barriers or equivalently insulating layers at the interfaces. As it has been shown above, the maximum feasibility of the focusing property occurs for $U \sim \mu$. However, in a practically wide range of barrier strengths, the focusing at least for the holes can be observed. Very commonly, an insulating layer is established due to the oxidation or mismatches in the electronic characters of the normal and superconducting layers. Therefore, it seems that controlling the barrier strength would be challenging. However, by changing the materials, different barrier strengths can be achieved [41,42] and it is even possible to have highly transparent interfaces such as Al/Au [12]. Therefore, choosing suitable materials for the two normal and the superconducting leads, different barrier strengths for the two interfaces, and particularly the extreme cases of NISN or NSIN structures with a single barrier can be achieved.

On top of the above-mentioned requirements, there are some other parameters including disorder or finite size in the $y$ direction which may affect the focusing character of the junction. Although it has not been considered explicitly here, however, similar to the graphene-based Veselago lenses, a finite disorder strength suppresses the focusing signals and the focal points are washed out and broadened by impurity scattering [35]. Hence it is crucial to have clean and almost impurity-free samples to see clear focusing patterns for holes and electrons. On the other hand, in NISIN junctions with a finite width in the vertical direction, the back reflection of electronic waves from the boundaries could lead to further interferences. But as long as this vertical width is large enough compared to $W$, $x_0$, and $\xi$, the intensity of the reflected waves will be much smaller than the focused waves coming from CAR. It is worth noting that the focus positions remain unchanged in the presence of a finite vertical width. In fact, as we can understand from the classical trajectories shown in Fig. 1, those with small enough angles will not see the boundaries before being focused by the S layer. All of these trajectories cross at the focal points and give rise to an intense focusing. However, the trajectories with larger angles will be reflected by the horizontal boundaries and, depending on their angles, they will pass through different points. Therefore, unless for very narrow junctions in which most of the electronic waves are reflected, the finite vertical width cannot strongly influence the focusing pattern.

Throughout the paper we have considered zero temperature, which simplifies the Green's function calculations, while at finite temperatures one needs to calculate a finite temperature Green's function which, technically speaking, needs to sum over Matsubara frequencies. But even without calculations it is possible to discuss the effect of temperature on focusing, based on a physical intuition. To this end we note that, according to our model and the obtained results, the excitation energy

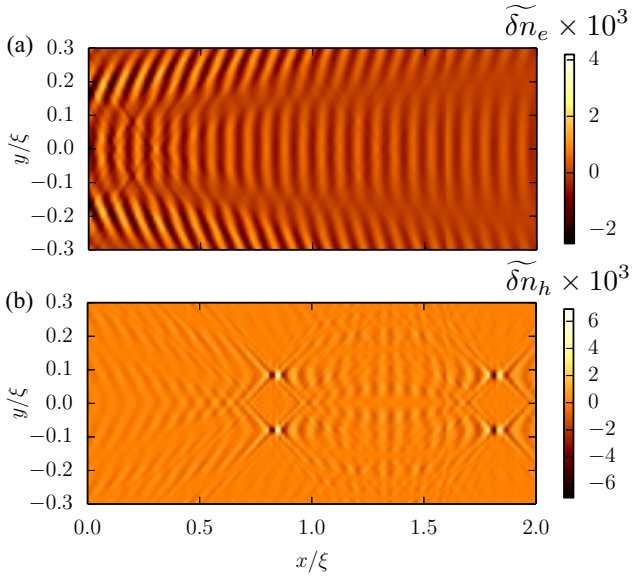


FIG. 7. Spatial variations of (a) electron and (b) hole densities inside the second normal contact $N_2$ when there are two injection points separated by $\delta y = 5\lambda_F$ in the $y$ direction. All parameters are the same as those used for Fig. 2. The corresponding focuses of each injection can be clearly seen beside the extra interferences of electron and hole waves induced by a two-point source.

can only slightly affect the CAR and EC signals. Moreover, due to the electron-hole symmetry as a basic character of superconductors, for all values of the excitation energy inside the superconducting gap ($|\epsilon| < \Delta_0$), the positions of focuses do not depend on $\epsilon$. This can be simply understood from the semiclassical arguments and the fact that the wave-vector dependence on $\epsilon$ is negligible. Now the main effect of temperature is to excite quasiparticles with energies below the thermal energy ($\epsilon \lesssim k_B T < \Delta_0$). Thus, as long as the S layer is in its superconducting state, most of the thermally excited quasiparticles will have subgap energies and all of them will be focused almost in the same way. So we can say in brief that due to the electron-hole symmetry as a basic characteristic of superconductors, the focusing properties of the junction cannot be influenced by thermal excitations when $T < T_c$, with $T_c$ indicating the critical temperature of the superconductor. As a result, there will not be any observable broadening of the focal points due to the finite temperature. This is in fact an advantage of the superconducting lens studied here in comparison with Veselago-like lenses in materials with chiral relativistic dispersion, such as graphene [35–37]. For instance, in the *p-n* junctions based on graphene, even when one considers a symmetric potential profile, only electrons and holes at the Fermi level have the same magnitude momenta. Then, in graphene-based Veselago lenses, the electron-hole symmetry is broken for excitations above the Fermi level. Hence, depending on the excitation energy, the focusing takes place in slightly different points, which leads to the broadening of the focuses at finite temperatures [36].

We finally comment on the possible experimental setups for the injection of electrons and the detection of the lensing effects. In order to inject electrons locally from a point source, one can either use a tip of a scanning tunneling microscope or, alternatively, a small submicron-sized gate with a size comparable to the Fermi wavelength or below it. Even for larger electron sources, the focusing would take place but in a broadened form of the focuses inside $N_2$. Although we have not considered this case explicitly, however, in order to understand the effect of a broad injection point, Fig. 7 shows the density variations in the presence of two point sources separated by $\delta y = 5\lambda_F$ in the vertical direction. We see that, irrespective of extra interferences, we will have well-separated focuses corresponding to each of the injection points. Therefore, we can simply expect similar imaging signatures for more injection points and even a broad electron source. Similar to the injection itself, the spatial variation of the electron and hole local currents and densities inside $N_2$ can be detected via scanning probe microscopes (SPMs) which have been already used for imaging electron motions in 2DEG [43,44].

## IV. CONCLUSIONS

In summary, we study the focusing of electron and hole excitations induced by CAR and multiple reflections from the interfaces of an NISIN junction when incoming electrons are locally injected inside the left metallic contact. It is shown that the barrier potentials at the interfaces intensify the focal points due to the CAR while suppressing the EC signal. In fact, the barrier potentials provide the required abrupt changes in particle momentum during a CAR. In addition, the intensities and the configuration of electron and hole focuses can be controlled by varying the location of the electron injector, width of the superconductor, and the potential barriers. These findings suggest promising applications of the superconducting lenses for remote manipulation of the entanglement in spatially separated electron or hole pairs.

## ACKNOWLEDGMENTS

We would like to acknowledge the encouragement and instructive comments of the late Malek Zareyan in the early stages of the work. H.C. and A.G.M. thank the International Center for Theoretical Physics (ICTP) for their hospitality and support during a visit in which part of this work was done. A.G.M. acknowledges financial support from Iran Science Elites Federation under Grant No. 11/66332.

[1] R. Horodecki, P. Horodecki, M. Horodecki, and K. Horodecki, Rev. Mod. Phys. **81**, 865 (2009).

[2] M. A. Nielsen and I. L. Chuang, *Quantum Computation and Quantum Information*, 10th ed. (Cambridge University Press, New York, 2011).

[3] G. Lesovik, T. Martin, and G. Blatter, Eur. Phys. J. B **24**, 287 (2001).

[4] P. Recher, E. V. Sukhorukov, and D. Loss, Phys. Rev. B **63**, 165314 (2001).

[5] J. M. Byers and M. E. Flatté, Phys. Rev. Lett. **74**, 306 (1995).

[6] G. Deutscher and D. Feinberg, Appl. Phys. Lett. **76**, 487 (2000).
[7] G. Deutscher, J. Supercond. **15**, 43 (2002).
[8] G. Falci, D. Feinberg, and F. W. J. Hekking, Europhys. Lett. **54**, 255 (2001).
[9] D. Feinberg, Eur. Phys. J. B **36**, 419 (2003).
[10] M. S. Kalenkov and A. D. Zaikin, Phys. Rev. B **75**, 172503 (2007).
[11] S. Russo, M. Kroug, T. M. Klapwijk, and A. F. Morpurgo, Phys. Rev. Lett. **95**, 027002 (2005).
[12] P. Cadden-Zimansky and V. Chandrasekhar, Phys. Rev. Lett. **97**, 237003 (2006).
[13] P. Cadden-Zimansky, J. Wei, and V. Chandrasekhar, Nat. Phys. **5**, 393 (2009).
[14] A. Kleine, A. Baumgartner, J. Trbovic, and C. Schönenberger, Europhys. Lett. **87**, 27011 (2009).
[15] L. Hofstetter, S. Csonka, J. Nygård, and C. Schönenberger, Nature (London) **461**, 960 (2009).
[16] L. G. Herrmann, F. Portier, P. Roche, A. L. Yeyati, T. Kontos, and C. Strunk, Phys. Rev. Lett. **104**, 026801 (2010).
[17] L. Hofstetter, S. Csonka, A. Baumgartner, G. Fülöp, S. d'Hollosy, J. Nygård, and C. Schönenberger, Phys. Rev. Lett. **107**, 136801 (2011).
[18] J. Schindele, A. Baumgartner, and C. Schönenberger, Phys. Rev. Lett. **109**, 157002 (2012).
[19] A. Das, Y. Ronen, M. Heiblum, D. Mahalu, A. V. Kretinin, and H. Shtrikman, Nat. Commun. **3**, 1165 (2012).
[20] T. Yamashita, S. Takahashi, and S. Maekawa, Phys. Rev. B **68**, 174504 (2003).
[21] D. Beckmann, H. B. Weber, and H. v. Löhneysen, Phys. Rev. Lett. **93**, 197003 (2004).
[22] P. Cadden-Zimansky, Z. Jiang, and V. Chandrasekhar, New J. Phys. **9**, 116 (2007).
[23] J. P. Morten, A. Brataas, and W. Belzig, Phys. Rev. B **74**, 214510 (2006).
[24] A. Brinkman and A. A. Golubov, Phys. Rev. B **74**, 214512 (2006).
[25] D. S. Golubev, M. S. Kalenkov, and A. D. Zaikin, Phys. Rev. Lett. **103**, 067006 (2009).
[26] D. Futterer, M. Governale, M. G. Pala, and J. König, Phys. Rev. B **79**, 054505 (2009).
[27] G. Michałek, B. R. Bułka, T. Domański, and K. I. Wysokiński, Phys. Rev. B **88**, 155425 (2013).
[28] J. Cayssol, Phys. Rev. Lett. **100**, 147001 (2008).
[29] J. Nilsson, A. R. Akhmerov, and C. W. J. Beenakker, Phys. Rev. Lett. **101**, 120403 (2008).
[30] J. Linder, M. Zareyan, and A. Sudbø, Phys. Rev. B **80**, 014513 (2009).
[31] H. Haugen, D. Huertas-Hernando, A. Brataas, and X. Waintal, Phys. Rev. B **81**, 174523 (2010).
[32] W. Chen, R. Shen, L. Sheng, B. G. Wang, and D. Y. Xing, Phys. Rev. B **84**, 115420 (2011).
[33] J. Linder and T. Yokoyama, Phys. Rev. B **89**, 020504 (2014).
[34] A. Schroer, P. G. Silvestrov, and P. Recher, Phys. Rev. B **92**, 241404 (2015).
[35] S. Gómez, P. Burset, W. J. Herrera, and A. L. Yeyati, Phys. Rev. B **85**, 115411 (2012).
[36] V. V. Cheianov, V. Fal'ko, and B. L. Altshuler, Science **315**, 1252 (2007).
[37] A. G. Moghaddam and M. Zareyan, Phys. Rev. Lett. **105**, 146803 (2010).
[38] A. L. Fetter and J. D. Walecka, *Quantum Theory of Many-Particle Systems* (Dover, New York, 2003).
[39] H. B. Heersche, P. Jarillo-Herrero, J. B. Oostinga, L. M. K. Vandersypen, and A. F. Morpurgo, Nature (London) **446**, 56 (2007).
[40] S.-Y. Xu *et al.*, Nat. Phys. **10**, 943 (2007).
[41] A. Kleine, A. Baumgartner, J. Trbovic, D. S. Golubev, A. D. Zaikin, and C. Schönenberger, Nanotechnology **21**, 274002 (2010).
[42] J. Fritzsche, R. B. G. Kramer, and V. V. Moshchalkov, Phys. Rev. B **80**, 094514 (2009).
[43] M. A. Topinka, B. J. LeRoy, R. M. Westervelt, S. E. J. Shaw, R. Fleischmann, E. J. Heller, K. D. Maranowski, and A. C. Gossard, Nature (London) **410**, 183 (2001).
[44] K. E. Aidala *et al.*, Nat. Phys. **3**, 464 (2007).